Nanoscale

ROYAL SOCIETY OF CHEMISTRY

COMMUNICATION

View Article Online
View Journal | View Issue

Cite this: *Nanoscale*, 2024, **16**, 2847

Received 21st November 2023,
Accepted 14th January 2024

DOI: 10.1039/d3nr05910c

rsc.li/nanoscale

Electroosmotic flow spin tracers near chemical nano/micromotors†

Donghao Cui, Zuyao Yan, Xiaowen Chen, Jiayu Liu and Wei Wang *

We report the first experimental observation of tracer spinning in place alongside chemically powered individual nano/micromotors. The torques are primarily generated by the electroosmotic flow on the motor surface. Such spinning is observed in various combinations of nano/micromotors and tracers of different shapes, sizes and chemical compositions.

Nano/micromotors are a unique class of colloidal particles that self-propel by converting energy stored in their environments into autonomous motion.[1] They interact with their environments through chemical gradients, electrostatics, and fluid flows.[2,3] For example, a passive colloidal particle (*i.e.*, a tracer) could move toward or away from a nano/micromotor by electrophoresis and/or diffusiophoresis.[4,5] A tracer can also be advected by the flows around a nano/micromotor or by the electro-/diffusio-osmotic flows on a substrate.[6] As a result, a nano/micromotor attracts or repels nearby tracers and forms exclusion zones,[6,7] colloidal crystals,[8,9] or colloidal gels.[10,11]

Beyond attraction and repulsion, torques are another primary interaction mechanism, and play a critical role in inducing collective behaviors among rod-shaped natural microswimmers.[12] Yet, torques by synthetic nano/micromotors are rarely reported. Two studies have shown circular advection of tracers along the $x(y)$–z plane at the edge of a cluster of chemical micromotors[16] and near a moving ion exchange resin particle,[17] respectively. In both cases, the torque is induced by a coupling between the gradient generated by the cluster/resin particle and a substrate. Whether an individual motor can generate torques that spin its neighbors and how they spin remain to be observed. Note that we are focusing on the torques exerted by a moving nano/micromotor on its neighbors, rather than on itself, which makes it a rotor that is beyond the scope of this work.[13–15]

We report in this communication that a chemically powered nano/micromotor spins nearby tracers, so that a tracer moves along with the nanomotor and spins in place (in the co-moving frame), unlike the tracers in ref. 16 and 17 that orbit in large convective loops. The nanomotors used in this study are bi-segmented gold–rhodium (Au–Rh) nanorods ~3–7 μm long and ~300 nm in diameter (Fig. 1a), made by template-assisted electrodeposition (see the ESI† for details). When placed in hydrogen peroxide (H_2O_2) aqueous solutions of typically 5 or 10 wt%, Au–Rh rods move toward their Rh ends at speeds on the order of 10 μm s^{-1}.[18] In addition, the leading end (Rh) of the nanomotor readily collected tracer microspheres (negatively charged SiO_2 microspheres, Fig. 1b), which is consistent with an earlier study.[19] Once close to the rod, the tracer sphere tended to be collected at the junction where two metals met (Fig. 1c).

The collected tracers moved with the nanomotor and spontaneously spun. Specifically, they typically spun about a tilted axis vertical to the long axis of the rod motor (see Fig. 1d for

School of Materials Science and Engineering, Harbin Institute of Technology (Shenzhen), Shenzhen, Guangdong 518055, China. E-mail: weiwangsz@hit.edu.cn

†Electronic supplementary information (ESI) available. See DOI: https://doi.org/10.1039/d3nr05910c

Wei Wang

Wei Wang received his BS from Harbin Institute of Technology (2008) and his PhD in Chemistry from Penn State University (2013) under the supervision of Prof. Thomas Mallouk. He is currently a full professor in the School of Materials Science and Engineering at Harbin Institute of Technology (Shenzhen), located in Shenzhen, China. Dr Wang's research laboratory works on experimental active colloids, with interests in their individual propulsion mechanisms, pairwise interactions, dynamics in complex environments, and collective behavior. A key mission is to understand and control colloidal active matter as well as emergent behaviors in other complex systems. Group website: https://weiwang-hitsz.weebly.com/.

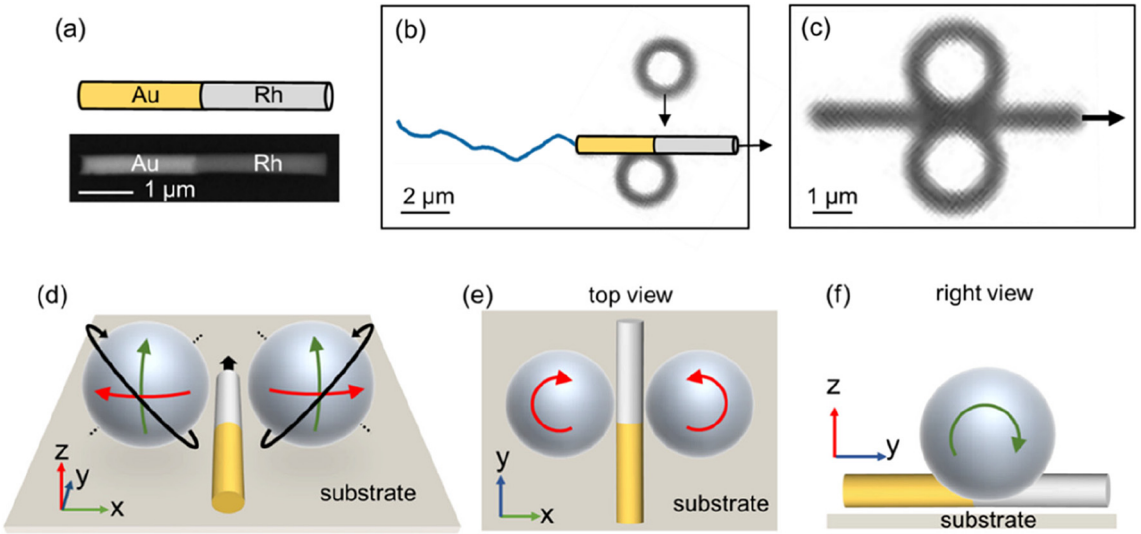

Fig. 1 Au–Rh nanorod motors collect and spin tracer microspheres. (a) Backscattered SEM image of an Au–Rh nanorod and its cartoon diagram. (b and c) Two SiO_2 microspheres 2 μm in diameter and zeta potential of −46 mV are attracted by a moving Au–Rh nanorod (b) and collected to the metal junction of the rod (c), in 5 wt% H_2O_2. (d) Schematic of the tracer microspheres on either side of a Au–Rh nanorod. Tracers spin about a tilted axis (dashed black lines) vertical to the long axis of the rod motor. The 3D spinning (black arrows) can be considered as a combination of spinning on the *xy* plane (e, red arrows) and spinning on the *yz* plane (f, green arrows). The exposure of optical micrographs in (b) and (c) has been greatly increased (to the point of overexposure) to improve the contrast without losing the microscopic detail or distorting the image. The same modification was applied to other optical micrographs in this article.

schematics). Such 3D spinning can be approximated as a combination of spinning on the *xy* plane (*i.e.*, the bottom substrate where both the rod and the tracers are located, Fig. 1e) and spinning on the *yz* plane (Fig. 1f). Footages of such 3D spinning are given in Fig. S7 and Video S1,† along with cartoon renderings. For simplicity, we will focus below only on the spinning of tracers on the *xy* plane because it is easier to visualize under a microscope with a fixed focus.

To quantitatively study the spinning of tracers on the *xy* plane, a SiO_2–Au Janus microsphere was chosen whose spinning was incidentally limited to the *xy* plane, presumably because of a weak attachment to the substrate (Fig. 2a and Video S2†). Under transmission optical microscope, such a Janus microsphere appears dark on the Au side and transparent on the SiO_2 side, thus providing the optical contrast to diffentiate its spinning. A close look reveals that such a Janus microsphere always spun clockwise/counterclockwise when collected at the left/right side of a nanorod motor moving toward its Rh end (Fig. 2b and c). Its spinning speed was on the order of 1 revolution per second (rps), and the spinning speed was largely constant in a cycle (Fig. 2d), suggesting that the Janus nature of the microsphere did not significantly affect its spinning. We therefore surmise that such spinning occurs generically for all tracer microspheres, Janus or not, but this is experimentally challenging to test because the spinning of isotropic spheres is difficult to tell. Note that one could test the spinning of a SiO_2–Au Janus microsphere that is further coated with a thin layer of SiO_2 on its Au hemisphere, so that the particles' surface chemistry is isotropic but its spinning is optically resolvable. However, we do not currently have access to these particles. In addition, the spinning speed increased monotonically with the fuel (H_2O_2) concentrations (Fig. 2e), suggesting that the rotation was related to the motor's motility. Finally, a moving nanorod motor can sequentially spin multiple spheres as it moves through them (Fig. 2f and Video S3†), suggesting that such spinning is not limited to particular spheres or specific positions of a motor or a sphere.

To understand the spinning of tracers near a moving nanorod motor, it is helpful to revisit its propulsion mechanism, popularly believed to be self-electrophoresis (Fig. 3a).[20] According to this mechanism, a bimetallic nanorod catalyzes the electrochemical decomposition of H_2O_2 so that H_2O_2 oxidizes on the anode (Rh) and reduces on the cathode (Au) end of the rod, respectively. This reaction produces H^+ and consumes it at Rh and Au, respectively, thus establishing an electric field that points from Rh to Au through the surrounding aqueous medium. This electric field pumps the charged fluid in the electrical double layer of the negatively charged nanorod toward the cathode (Au) so the rod moves toward the anode (Rh). Fig. 3b shows the results from numerical simulation of the distributions of the electrical potential and flows near such a bimetallic nanorod motor.

Besides enabling propulsion, the self-generated electric field of an Au–Rh motor also attracts negatively charged tracers to the Rh end and repels them away from the Au end (Fig. 3c), which is essentially electrophoresis.[19] More subtly, because the electric field is spatially nonuniform and strongest at the rod junction where two metals meet, positively polarizable tracers (as they are in our experiments) that are already electrically attracted to the vicinity of a nanomotor are further

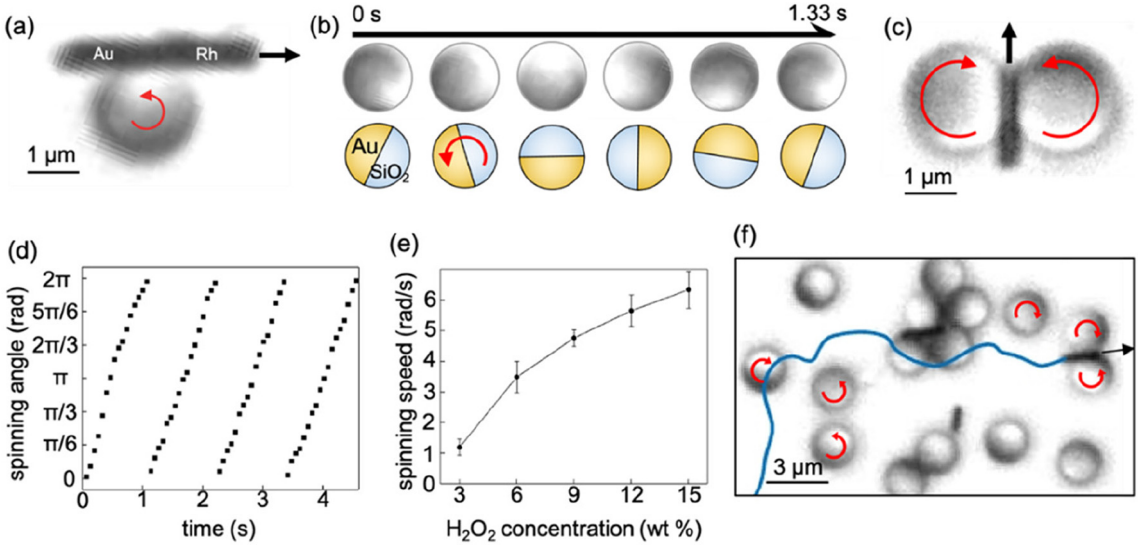

Fig. 2 A closer examination of the spinning of SiO_2–Au Janus microspheres near an Au–Rh nanorod motor. (a and b) A SiO_2–Au Janus microsphere spinning on the *xy* plane (a), taken from Video S2.† The orientations of the SiO_2–Au Janus microsphere over time are shown in (b) as optical micrographs (top) and cartoons (bottom). (c) The microspheres collected to the right (left) side of a nanorod spun counterclockwise (clockwise). (d) Change in the angle of a spinning SiO_2–Au Janus microsphere over time. The spinning angle is defined as the angle between the *x* axis and the line pointing from the center of the dark to the bright hemispheres of a Janus microsphere. Experiments were performed in 5 wt% H_2O_2. (e) The angular speed of a spinning SiO_2–Au Janus microsphere at different fuel (H_2O_2) concentrations. (f) An Au–Rh nanorod spun multiple SiO_2–Au Janus microspheres as it moved through them (motor trajectory shown as blue line), taken from Video S3.†

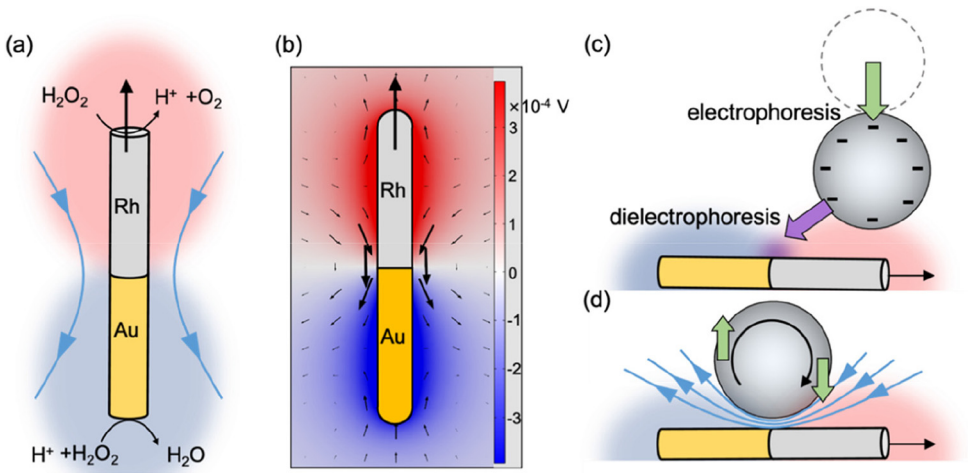

Fig. 3 The mechanism of the collection and spinning of SiO_2–Au Janus microspheres by an Au–Rh nanorod motor. (a and b) Schematic diagram (a) and numerical simulation (b) of the electric potential (colors) and fluid flows (arrows) around an Au–Rh nanorod in the lab frame. The sizes of the arrows are proportional to the flow magnitude. (c) Schematic of a negatively charged SiO_2–Au Janus microsphere being collected to a nanorod motor *via* the combined effect of electrophoresis and dielectrophoresis. (d) Schematic of a negatively charged a SiO_2–Au Janus microsphere spinning near a nanorod motor *via* torques produced by electrostatics (green arrows) and flows (blue arrows).

attracted to the rod junction *via* dielectrophoresis (Fig. S3b†), as recently argued by ref. 21. This dielectrophoretic force, along with the electrophoretic force that attracts the tracer to the nanorod ends, holds the tracer in place against the local flows while it co-moves with a nanorod motor.

Furthermore, this self-generated electric field also spins a tracer by electrostatics and flows (Fig. 3d). First, a negatively charged tracer held to the side of a nanorod motor responds to this electric field electrostatically, so that its charged body is electrically pulled and pushed by the Rh and Au end of the rod, respectively. This leads to an electrostatic torque of 1.4×10^{-22} N m for a 3 μm SiO_2 microsphere near a 3 μm Au–Rh nanorod motor in 5 wt% H_2O_2, as suggested by finite element simulations (see the ESI† for simulation details).

On the other hand, the electroosmotic flow around a nanomotor, arising from the coupling between the self-generated

electric field and a negatively charged nanorod surface, is distributed so that fluid flows from the bulk toward the Rh end, along the rod surface, then outward to the bulk from the Au end, with a peak in flow magnitudes at the metal junction. As a result, this flow (shown in Fig. 3b) advects a tracer held at the junction into rotation, with a hydrodynamic torque that is equal in sign but 4 orders of magnitude larger (2.6×10^{-19} N m) than the electrostatic torque described above. Simulations and experiments also showed that tracers of different surface zeta potentials (Fig. S9†), or those with nonuniform surface charge distributions (Fig. S10†), spun at similar speeds. These results collectively suggest that hydrodynamic torques dominate in causing a tracer sphere to spin near a nanorod motor. Quantitatively, this hydrodynamic torque is predicted to spin a tracer at 1.7 rps, calculated by Stokes' law with a reasonable surface proton flux of 7×10^{-6} mol $(m^2\ s)^{-1}$,[22] which agrees well with the experimental value of 1 rps.

We briefly discuss the role of a substrate in the observed spinning of tracers. Up to this point, our simulations have only considered the spinning of tracers on the *xy* plane, and have assumed the absence of a substrate and that the nanorod and the sphere are of the same height. A more complete model considering 3D spinning and realistic positions of a rod–sphere pair on a substrate is given in Fig. S6,† and agrees qualitatively with results presented above as well as experimental observations (Fig. S7†). In these simulations, the key factor for the spinning of a tracer on the *xz* or *yz* plane (rather than the *xy* plane discussed above) is a difference in the heights between a motor and a tracer, and in the heights between them and the substrate. On the other hand, a substrate is not necessary for the spinning of tracers on the *xy* plane (confirmed by simulation in Fig. S11†) because neither the electrostatic nor the hydrodynamic torque described above requires a substrate. Therefore, we expect qualitatively the same spinning to occur even if experiments were performed in the bulk fluid far from any boundary (experiments not performed due to technical difficulty) but perhaps with different spinning speeds.

The spinning of tracers is a common feature found for motors and tracers of different shapes, sizes and compositions. For example, Fig. 4a shows that a gold nanorod (immotile in H_2O_2, thus a tracer) swung its body when a bimetallic nanorod motor passed by (Video S4†). Fig. 4b shows that larger tracer spheres spin more slowly than smaller ones (Video S5; see Fig. S8a† for data). Conversely, Fig. S8b† shows that larger micromotors spin tracers more slowly. Fig. 4c shows the spinning of multiple SiO_2 tracers near SiO_2–Pt[23] or Au–Pt spherical micromotors,[24,25] or near photochemical TiO_2–Pt spherical micromotors[26] (Video S6†). Finally, Fig. 4d shows that oil droplets (dibutyl phthalate) also spin near SiO_2–Pt micromotors (Video S7†). In addition, we further speculate that because shear flows are common for nano/micromotors,[27] tracers could also spin near motors powered by electromagnetic waves, heat, light, or ultrasound. However, such spinning

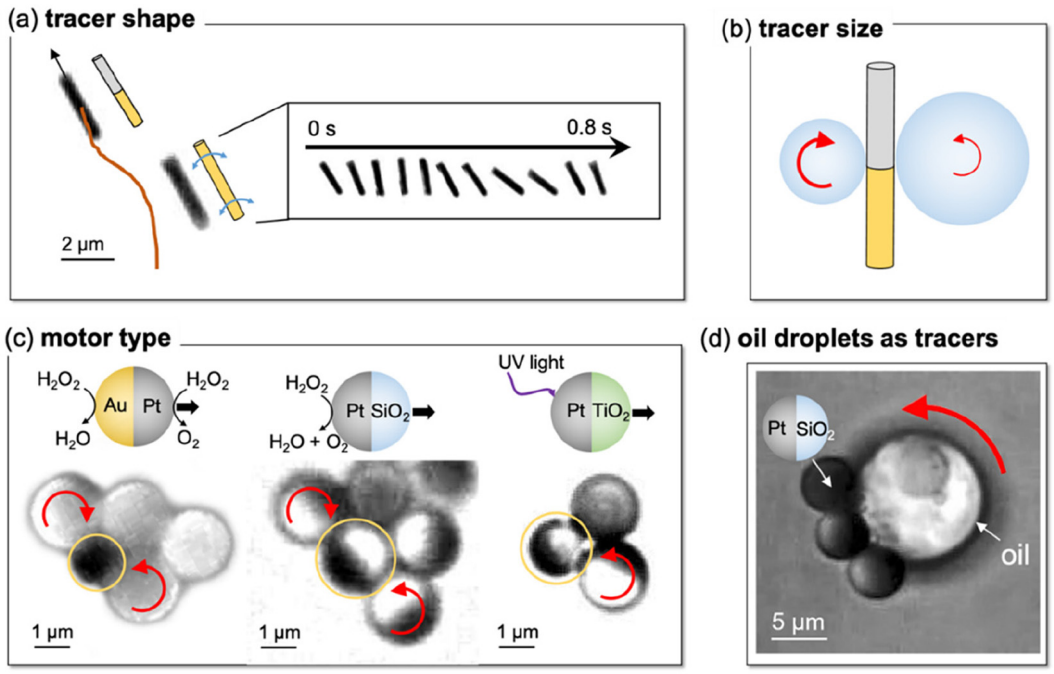

Fig. 4 Tracers spinning near a micro/nanomotor is a common feature. (a) An immotile gold nanorod swung during the passage of a nearby Au–Rh nanorod motor in 5 wt% H_2O_2, taken from Video S4.† Inset: Time-elapsed optical micrographs of the gold nanorod. (b) Schematic showing that larger tracers spin more slowly than smaller tracers. See Video S5† for actual footage and Fig. S8† for data. (c) Multiple SiO_2–Au Janus microspheres spinning near (from left to right) SiO_2–Pt, Au–Pt, and photocatalytic TiO_2–Pt spherical micromotors, taken from Video S6.† The motor in each case is circled in yellow. (d) An oil droplet (dibutyl phthalate) spinning near a chemically powered SiO_2–Pt micromotor, taken from Video S7.† Experiments in (c) and (d) were in 10 wt% H_2O_2.

can be difficult to visualize because the spinning of Janus tracers could in one way or another be interfered by these external fields.

In conclusion, although rotating tracers have been reported before,[16,17] we have reported the first observation of tracers spinning in place near a single nano/micromotor. A tracer is first collected and held to the side of a motor *via* electrophoresis and dielectrophoresis. It then spins by the torques from both electrostatics and from the electroosmotic flows near the motor surface, with the latter dominating. Such spinning of tracers near nano/micromotors is a universal feature found in different combinations of chemically powered nanomotors and tracers of different shapes, sizes and chemical compositions. Beyond the typically considered attraction and repulsion, this study reveals the important role of torques in the interactions between nano/micromotors and their surroundings, even at a single motor level. These findings could help understand the collective behaviors among nano/micromotors, and lead to new avenues of micro-assembly and microfabrication that is enabled by torques.

Conflicts of interest

There are no conflicts to declare.

Acknowledgements

This project was financially supported by the National Natural Science Foundation of China (T2322006) and the Shenzhen Science and Technology Program (RCYX20210609103122038 and JCYJ20210324121408022).

Notes and references

1 X. Chen, C. Zhou and W. Wang, *Chem. – Asian J.*, 2019, **14**, 2388–2405.
2 L. Wang and J. Simmchen, *Condens. Matter*, 2019, **4**, 78.
3 M. N. Popescu, W. E. Uspal, A. Domínguez and S. Dietrich, *Acc. Chem. Res.*, 2018, **51**, 2991–2997.
4 C. Zhou, H. P. Zhang, J. Tang and W. Wang, *Langmuir*, 2018, **34**, 3289–3295.
5 D. Velegol, A. Garg, R. Guha, A. Kar and M. Kumar, *Soft Matter*, 2016, **12**, 4686–4703.
6 C. Wu, J. Dai, X. Li, L. Gao, J. Wang, J. Liu, J. Zheng, X. Zhan, J. Chen, X. Cheng, M. Yang and J. Tang, *Nat. Nanotechnol.*, 2021, **16**, 288–295.
7 X. Chang, C. Chen, J. Li, X. Lu, Y. Liang, D. Zhou, H. Wang, G. Zhang, T. Li, J. Wang and L. Li, *ACS Appl. Mater. Interfaces*, 2019, **11**, 28507–28514.
8 I. D. Hosein and C. M. Liddell, *Langmuir*, 2007, **23**, 8810–8814.
9 B. Li, D. Zhou and Y. Han, *Nat. Rev. Mater.*, 2016, **1**, 15011.
10 S. A. Mallory, M. L. Bowers and A. Cacciuto, *J. Chem. Phys.*, 2020, **153**, 084901.
11 M. E. Szakasits, W. Zhang and M. J. Solomon, *Phys. Rev. Lett.*, 2017, **119**, 058001.
12 M. Bär, R. Großmann, S. Heidenreich and F. Peruani, *Annu. Rev. Condens. Matter Phys.*, 2020, **11**, 441–466.
13 R. Niu and T. Palberg, *Soft Matter*, 2018, **14**, 7554–7568.
14 B. Liebchen and D. Levis, *EPL*, 2022, **139**, 67001.
15 X. Lyu, J. Chen, R. Zhu, J. Liu, L. Fu, J. L. Moran and W. Wang, *ACS Nano*, 2023, **17**, 11969–11993.
16 S. A. Nabavizadeh, J. Castañeda, J. G. Gibbs and A. Nourhani, *Part. Part. Syst. Charact.*, 2022, **39**, 2100232.
17 R. Niu, D. Botin, J. Weber, A. Reinmüller and T. Palberg, *Langmuir*, 2017, **33**, 3450–3457.
18 W. F. Paxton, K. C. Kistler, C. C. Olmeda, A. Sen, S. K. St. Angelo, Y. Cao, T. E. Mallouk, P. E. Lammert and V. H. Crespi, *J. Am. Chem. Soc.*, 2004, **126**, 13424–13431.
19 W. Wang, W. Duan, A. Sen and T. E. Mallouk, *Proc. Natl. Acad. Sci. U. S. A.*, 2013, **110**, 17744–17749.
20 Y. Wang, R. M. Hernandez, D. J. Bartlett, J. M. Bingham, T. R. Kline, A. Sen and T. E. Mallouk, *Langmuir*, 2006, **22**, 10451–10456.
21 A. A. Ashaju, J. A. Wood and R. G. H. Lammertink, *Langmuir*, 2022, **38**, 3040–3050.
22 W. F. Paxton, P. T. Baker, T. R. Kline, Y. Wang, T. E. Mallouk and A. Sen, *J. Am. Chem. Soc.*, 2006, **128**, 14881–14888.
23 J. R. Howse, R. A. L. Jones, A. J. Ryan, T. Gough, R. Vafabakhsh and R. Golestanian, *Phys. Rev. Lett.*, 2007, **99**, 048102.
24 I. Theurkauff, C. Cottin-Bizonne, J. Palacci, C. Ybert and L. Bocquet, *Phys. Rev. Lett.*, 2012, **108**, 268303.
25 P. M. Wheat, N. A. Marine, J. L. Moran and J. D. Posner, *Langmuir*, 2010, **26**, 13052–13055.
26 R. Dong, Q. Zhang, W. Gao, A. Pei and B. Ren, *ACS Nano*, 2016, **10**, 839–844.
27 A. I. Campbell, S. J. Ebbens, P. Illien and R. Golestanian, *Nat. Commun.*, 2019, **10**, 3952.